Bose metal in an exactly solvable model with infinite-range Hatsugai-Kohmoto interaction

Wei-Wei Yang [1], Hong-Gang Luo,[1,2,3] and Yin Zhong [1,3,*]

[1]*Key Laboratory of Quantum Theory and Applications of MoE & School of Physical Science and Technology, Lanzhou University, Lanzhou 730000, People's Republic of China*

[2]*Beijing Computational Science Research Center, Beijing 100084, People's Republic of China*

[3]*Lanzhou Center for Theoretical Physics, Key Laboratory of Theoretical Physics of Gansu Province, Lanzhou University, Lanzhou 730000, People's Republic of China*

In a conventional boson system, the ground state can either be an insulator or a superfluid (SF) due to the duality between particle number and phase. This paper reveals that the long-sought Bose metal (BM) state can be realized in an exactly solvable interacting bosonic model, i.e., the Bose-Hatsugai-Kohmoto (BHK) model, which acts as the nontrivial extension of Bose-Hubbard (BH) model. By tuning the parameters such as bandwidth W, chemical potential μ, and interaction strength U, a BM state without any symmetry breaking can be accessed for a generic W/U ratio, while a Mott insulator (MI) with integer boson density is observed at small W/U. The quantum phase transition between the MI and BM states belongs to the universality class of the Lifshitz transition, which is further confirmed by analyzing the momentum-distribution function, the Drude weight, and the SF weight. Additionally, our investigation at finite temperature reveals similarities between the BM state and the Fermi liquid, such as a linear-T dependent heat capacity ($Cv \sim \gamma T$) and a saturated charge susceptibility ($\chi_c \sim$ constant) as T approaches zero. Comparing the BM state with the SF state in the standard BH model, we find that the key feature of the BM state is a compressible total wavefunction accompanied by an incompressible zero-momentum component. Given that the BM state prevails over the SF state at any finite U in the BHK model, our paper suggests the possibility of realizing the BM state with on-site repulsion interactions in momentum space.

I. INTRODUCTION

In traditional interacting boson systems, bosons manifest as eigenstates of either the phase operator or the particle number operator, which correspond to superfluid (SF) [1] and insulating states [2], respectively. Within the well-known Bose-Hubbard (BH) model incorporating on-site interaction, bosons with weak interaction typically yield a SF state, while stronger interactions coupled with integer boson filling result in a bosonic Mott insulator (MI) that reinstates $U(1)$ symmetry [3]. Not only the Bose-Hubbard model with on-site interactions in real space exhibits such behavior, but also similar SF-MI phase transitions have been observed in the Bose-Hatsugai-Kohmoto (BHK) model [4], where on-site interactions are present in momentum space. Introducing disorder can trigger the appearance of a Bose glass exhibiting replica symmetry breaking [5]. However, in both circumstances, a metallic state does not readily emerge during the SF-MI transition. Furthermore, the no-go theorem—specifically the "Gang of four" scaling theory of localization—states the absence of metallic states in a two-dimensional system that involves disorder [6]. Consequently, identifying the presence of a metallic state in low-dimensional boson systems appears elusive and challenging.

Remarkably, an anomalous metallic state exhibiting residual resistance significantly lower than the quantum resistance (h/e^2) at low temperatures has been observed experimentally [7–21]. This metallic state is speculated to occur between superconducting and insulating states under specific conditions: the tuning of thinness, magnetic field, or gate voltage in superconducting films, Josephson-junction arrays, and superconducting islands [17,22–37]. Further experiments have observed the charge-2e quantum oscillation [20] and vanished Hall resistivity [16], which suggest that bosonic particles, i.e. the Cooper pair formed by two electrons, should play a decisive role in the anomalous metallic state between superconducting and insulating states. Therefore, the metallic states with bosonic nature has been identified as the Bose metal (BM) [17,27], which could potentially provide an explanation for these unusual metallic states themselves.

BM, as a common trend in the field of condensed matter physics, has stimulated numerous interesting theories, such as the phase glass, fractionalization, dissipation effect, vortex liquid, quantum Boltzmann theory, and the composite fermions [9,17,22–35,38–40]. An intriguing proposal suggests BM may exhibit behaviors akin to a Fermi liquid, with a Bose surface (comparable to the Fermi surface for fermions) where the excitation energy diminishes and gapless excitations naturally occur [38,39]. Contrary to the Fermi surface, the Bose surface does not demarcate the boundary between occupied and unoccupied states. However, despite many years

*zhongy@lzu.edu.cn

235149-1

of research, due to the complex interplay of correlation, disorder and magnetic field, the existing theories on this subject are often based on approximations that are difficult to control, such as mean-field decoupling, Gaussian effective action and slave-particle splitting with only large-N limit. (Note, however, some numerical evidences on BM with Bose surface supplemented with frustrated interaction [41,42].) Therefore, the underlying mechanisms behind the anomalous metal phenomenon are still not fully understood, which makes it an ongoing topic of investigation in condensed matter physics [17].

Given the challenges posed by BM states, we propose a simpler question: Is it feasible to identify an exactly solvable model that demonstrates BM as its ground state? Obviously, such thinking is motivated by recent progress on many solvable models, ranging from Kitaev's toric code, honeycomb lattice model to Sachdev-Ye-Kitaev model, and Hatsugai-Kohmoto (HK) model [43–54]. These models have yielded intriguing quantum spin liquids and non-Fermi liquids, enhancing our understanding of spin liquids with Majorana fermion excitation and non-Fermi liquids without quasiparticle in the presence of dominant disordered interaction.

In the present study, we uncover a BM state by reinvestigating an exactly solvable model with infinite-range interaction, namely, the BHK model [4]. It is crucial to note that the BHK model serves as the bosonic counterpart to the extensively researched HK model [55–69]. (Note, however, that the main results of the single-band HK model were established earlier by an intriguing theory known as the superexclusion statistics theory [70–72].) Thanks to its infinite-range interaction, the BHK model can be diagonalized in momentum space, revealing the emergence of the BM state for any finite interaction strength, in contrast to the SF state. The identification of the BM state is corroborated by several distinctive characteristics, including a unique momentum distribution function, a finite Drude weight, and a vanishing SF weight. The BM state in the BHK model exhibits several properties reminiscent of a conventional Fermi liquid, such as the Bose surface, a linear temperature-dependent heat capacity, and the saturation of charge susceptibility at low temperatures. The transition from the MI to the BM phase, driven by band filling, belongs to the universality class of the Lifshitz transition, commonly observed in noninteracting fermionic systems. It warrants emphasis that the SF state only occurs in the noninteracting limit, indicating that the on-site interaction in momentum space (or infinite-range interaction in real space) is sufficient and crucial for the formation of the BM state. Importantly, our identified BM state does not rely on the presence of disorder, external magnetic field, or fine tuning of carrier density. Therefore, the BM state could be considered as a new fixed point of interacting Bose systems. For now, the realization of long-range interactions in specific materials remains elusive. However, there is a potential avenue for achieving such interactions through the creation of a synthetic lattice composed of momentum states [73–83].

The subsequent sections of this paper are structured as follows. Section II serves as an introduction to the BHK model, highlighting the key observables employed in the investigation of this model, including the single-particle

spectral function $A(k, \omega)$, the Drude weight, the SF weight, and the charge susceptibility. Section III presents the results obtained in this study, encompassing the properties of the phase diagram, the MI state, the BM state, and the MI-BM Lifshitz transition at zero temperature. Section IV delves into the finite-temperature properties, focusing on the heat capacity and charge susceptibility. Section V further explores the band structure and compressibility, drawing comparisons with the SF state observed in the BH model. Additionally, the resemblance between the BM state and the Fermi liquid is elucidated in the limit of $U \to \infty$. Finally, Sec. VI provides a summary of the findings of this paper.

II. THE MODEL

We consider the following BHK model, which is defined for interacting bosons on a lattice,

$$
\hat{H} = -\sum_{i,j} t_{ij} \hat{c}_i^\dagger \hat{c}_j - \mu \sum_j \hat{c}_j^\dagger \hat{c}_j
$$
$$
+ \frac{U}{2N_s} \sum_{j_1,j_2,j_3,j_4} \delta_{j_1+j_3=j_2+j_4} \hat{c}_{j_1}^\dagger \hat{c}_{j_3}^\dagger \hat{c}_{j_2} \hat{c}_{j_4}. \quad (1)
$$

Here, $\hat{c}_j^\dagger$ is the creation operator of boson at site j and it satisfies commutative relation $[\hat{c}_i, \hat{c}_j^\dagger] = \delta_{ij}$. t_{ij} denotes the hopping integral between i, j sites and has translation invariance, i.e., $t_{ij} = t_{i-j}$. We consider a grand-canonical ensemble and the number of bosons can be tuned by varying chemical potential μ. N_s is the number of lattice sites. The last term in Hamiltonian is the HK interaction, which is infinite ranged between any four bosons but preserves the center of motion (embodied by the constraint of the δ function). It should be emphasized that all nontrivial physics come from this interaction since it stabilize a new fixed point [61].

Since the HK interaction is local in momentum space, a Fourier transformation on the original Hamiltonian (1) leads to

$$
\hat{H} = \sum_k \hat{H}_k = \sum_k \left[\epsilon_k \hat{n}_k + \frac{U}{2} \hat{n}_k(\hat{n}_k - 1) - \mu \hat{n}_k \right], \quad (2)
$$

where $\hat{n}_k = \hat{c}_k^\dagger \hat{c}_k$ is the number of bosons in a state labeled by momentum k. It is interesting to note that since $[\hat{H}_k, \hat{H}_{k'}] = 0$ for any k, k', the BHK model is a frustration-free model but can have nontrivial physics if each sector $\hat{H}_k$ is not trivial [84]. For simplicity, we consider our system is on hypercubic lattice with only nearest-neighbor hopping t, so the dispersion of bosons is $\epsilon_k = -2t \sum_{i=1}^d \cos k_i$.

To solve Eq. (2), we observe that in each $\hat{H}_k$, $\hat{n}_k$ is a good quantum number, thus if we choose $\hat{n}_k$'s eigenstate $|n_k\rangle$ ($n_k = 0, 1, 2, ...$) as basis, $\hat{H}_k$ is automatically diagonalized with its eigenenergy

$$
E_{n_k} = (\epsilon_k - \mu)n_k + \frac{U}{2}n_k(n_k - 1). \quad (3)
$$

Particularly, the ground state of $\hat{H}_k$ is determined by minimizing E_{n_k}, i.e., $\frac{\partial E_{n_k}}{\partial n_k} = 0$, which gives $n_k = \text{int}[\frac{1}{2} + \frac{\mu - \varepsilon_k}{U}]$ (int[x] gives the integer nearest to x). For the whole

Hamiltonian $\hat{H}$, its eigenstate is just the product-state of each $|n_k\rangle$,

$$\left| n_{k_1}, n_{k_2}, ..., n_{k_{N_s}} \right\rangle \equiv \left(\hat{c}_{k_1}^\dagger\right)^{n_{k_1}} \left(\hat{c}_{k_2}^\dagger\right)^{n_{k_2}} ... \left(\hat{c}_{k_{N_s}}^\dagger\right)^{n_{k_{N_s}}} |0,0,0...\rangle. \quad (4)$$

Thus, without much effort, we have obtained all eigenstates of BHK model, which is a key feature of HK-like models.

Most importantly, the ground state of BHK model can be succinctly expressed as

$$|\Psi_g\rangle = \prod_{k\in\Omega_0} |0\rangle_k \prod_{k\in\Omega_1} |1\rangle_k ... \prod_{k\in\Omega_n} |n\rangle_k, \quad (5)$$

where Ω_n represents the momentum space regions with an occupancy of $\langle \hat{n}_k \rangle = n$ ($n = 0, 1, 2, 3...$). In the subsequent sections of this study, we will be guided by this simple ground-state wavefunction and employ various physical observables, such as the particle distribution function, single-particle spectrum function, Drude weight, SF weight, and charge susceptibility, to construct the phase diagram of the BHK model.

A. Single-particle Green's function and spectral function

Firstly, let us define the single-particle (boson) retarded Green's function

$$G^R(t, k) = -i\theta(t)\langle [\hat{c}_k(t), \hat{c}_k^\dagger] \rangle = -i\theta(t) \frac{\text{Tr}(e^{-\beta\hat{H}} [\hat{c}_k(t), \hat{c}_k^\dagger])}{\mathcal{Z}}.$$

Here, $\theta(t)$ is the unit step function with $\theta(t) = 1$ for $t > 0$ and vanishes for $t < 0$. $\mathcal{Z} = \text{Tr} e^{-\beta\hat{H}} = \prod_k \mathcal{Z}_k = \prod_k \sum_{n_k=0}^\infty e^{-\beta E_{n_k}}$ is the partition function. We note that in contrast to the case in standard HK model for fermion, here, the summation over n_k cannot be performed analytically and numerical calculation with cutoff (define a maximum for n_k) has to be used. Then, armed with eigenstate Eq. (4), eigen-energy Eq. (3), we have derived the retarded Green's function $G^R(\omega, k)$ in terms of the Lehmann spectral representation,

$$
\begin{aligned}
G^R(\omega, k) &= \int_{-\infty}^\infty dt\, e^{i(\omega+i0^+)t} G^R(t, k) \\
&= \sum_{n_k, m_k} \frac{e^{-\beta E_{n_k}}}{\mathcal{Z}_k} \left[\frac{|\langle n_k|\hat{c}_k|m_k\rangle|^2}{\omega + i0^+ + E_{n_k} - E_{m_k}} \right. \\
&\quad \left. - \frac{|\langle n_k|\hat{c}_k^\dagger|m_k\rangle|^2}{\omega + i0^+ + E_{m_k} - E_{n_k}} \right] \\
&= \sum_{n_k} \frac{e^{-\beta E_{n_k}}}{\mathcal{Z}_k} \left[\frac{n_k + 1}{\omega + i0^+ + E_{n_k} - E_{n_k+1}} \right. \\
&\quad \left. - \frac{n_k}{\omega + i0^+ + E_{n_k-1} - E_{n_k}} \right].
\end{aligned}
$$

Obviously, when $T = 0$ only the excitation above the ground state contributes to the G^R. Thus, the summation over all n_k can be neglected and only the term with the ground-state particle occupation $n_k = n_k^0$ is preserved. So, we find the retarded

Green's function reduces to an analytical form

$$
\begin{aligned}
G^R(\omega, k) &= \frac{n_k^0 + 1}{\omega - (\varepsilon_k + U n_k^0 - \mu)} \\
&\quad - \frac{n_k^0}{\omega - (\varepsilon_k + U(n_k^0 - 1) - \mu)}, \quad (6)
\end{aligned}
$$

which is similar to the counterpart in the fermionic HK model $G^R(\omega, k) = \frac{1-n_k^0}{\omega-(\varepsilon_k-\mu)} + \frac{n_k^0}{\omega-(\varepsilon_k+U-\mu)}$ [66]. The first (second) term in Eq. (6) describes particle (hole) excitation with excitation energy $\omega_p = \varepsilon_k + U n_k^0 - \mu$ ($\omega_h = \mu - \varepsilon_k - U(n_k^0 - 1)$).

Then, we can obtain the spectral function $A(k, \omega)$ using the relation $A(k, \omega) = -\frac{1}{\pi}\text{Im}G^R(k, \omega + i0^+)$. This relation allows us to extract valuable information about the system's single-particle excitations and their energy distribution. It is important to note that $A(k, \omega)$ is positive for $\omega > 0$ and negative for $\omega < 0$. In Fig. 5 (see below), we present examples of $A(k, \omega)$, which will be further analyzed later.

B. Drude weight and superfluid weight

Next, following the general strategy of many-body physics to distinguish metallic and insulating states, we try to calculate the Drude weight and SF weight, which are the most relevant transport quantities [85,86]. The Drude weight D and SF weight D_s can be deduced by studying two different limiting behaviors of the current-current correlation function $\chi_{j_x j_x}(\mathbf{q}, \omega)$, which represents the paramagnetic component of the linear-current-response induced by the vector potential $A_x(\mathbf{q}, \omega)$,

$$\langle j_x(\mathbf{q}, \omega) \rangle = -[e^2(\langle -K_x \rangle - \chi_{j_x j_x}(\mathbf{q}, \omega))A_x(\mathbf{q}, \omega)], \quad (7)$$

$$\chi_{j_x j_x}(\mathbf{q}, \omega) \equiv \frac{i}{N_s} \int_{-\infty}^\infty dt\, \theta(t)\langle [j_x^p(\mathbf{q}, t), j_x^p(-\mathbf{q}, 0)] \rangle e^{i\omega t}. \quad (8)$$

The first term of Eq. (7) is the diamagnetic term, which contributes from the kinetic energy per site divided by the number of dimensions, i.e., $K_x = -\frac{t}{N_s} \sum_j (c_{j+x}^\dagger c_j + c_j^\dagger c_{j+x})$. The paramagnetic current is defined by $j_x^p(\mathbf{q}) = -it \sum_j e^{-i\mathbf{q}\cdot\mathbf{R}_j}(c_j^\dagger c_{j+x} - c_{j+x}^\dagger c_j)$.

The Drude weight is given by the δ-function part of the uniform conductivity $\sigma_{xx}(\omega) \equiv -e^2 \frac{\langle -K_x \rangle - \chi_{j_x j_x}(\mathbf{q}=\mathbf{0},\omega)}{i\omega}$ as $\omega \to 0$,

$$\frac{D}{\pi e^2} = \langle -K_x \rangle - \chi_{j_x j_x}(\mathbf{q} = \mathbf{0}, \omega \to 0). \quad (9)$$

If the order in which $\mathbf{q}$ and ω approach zeros is exchanged, one obtains the SF weight

$$\frac{D_s}{\pi} = \langle -K_x \rangle - \chi_{j_x j_x}(\mathbf{q} \to 0, \omega = 0). \quad (10)$$

Here we assume $q_x = 0$ for the $\mathbf{q} \to \mathbf{0}$ limit, since the London gauge requires that $\mathbf{q} \cdot \mathbf{A} = 0$. The current-current correlation function in the $q_x = 0$ situation can be written in a

compact way

$$
\chi_{j_x j_x}(\mathbf{q}, \omega)
$$

$$
= \frac{i}{N_s} \int_{-\infty}^{\infty} dt\, e^{i\omega t} \theta(t) \langle [j_x(\mathbf{q}, t), j_x(-\mathbf{q}, 0)] \rangle
$$

$$
= -i \frac{t^2}{N_s} \sum_{k_1, k_2} (e^{-i2k_x} + e^{i2k_x} - 2)
$$

$$
\times \int_{-\infty}^{\infty} dt\, e^{i\omega t} \theta(t) \langle [c_{\mathbf{k_1}}^{\dagger}(t) c_{\mathbf{k_1}+\mathbf{q}}(t), c_{\mathbf{k_2}}^{\dagger}(0) c_{\mathbf{k_2}-\mathbf{q}}(0)] \rangle
$$

$$
= \frac{t^2}{N_s} \sum_{\mathbf{k_1}, \mathbf{k_2}} (e^{-i2k_x} + e^{i2k_x} - 2) \ll c_{\mathbf{k_1}}^{\dagger} c_{\mathbf{k_1}+\mathbf{q}} \mid c_{\mathbf{k_2}}^{\dagger} c_{\mathbf{k_2}-\mathbf{q}} \gg_{\omega},
$$
(11)

where $\ll c_{\mathbf{k_1}}^{\dagger} c_{\mathbf{k_1}+\mathbf{q}} \mid c_{\mathbf{k_2}}^{\dagger} c_{\mathbf{k_2}-\mathbf{q}} \gg_{\omega}$ is the retarded Green's function in real-frequency domain. Here, considering $q_x = 0$, we omit the index of k_x and simply set $k_x = k_{1x} = k_{2x}$.

We first focus on the Drude weight [Eq. (9)]. The current-current correlation function now is simplified as

$$
\chi_{j_x j_x}(\mathbf{q} = \mathbf{0}, \omega \to 0)
$$

$$
= \frac{t^2}{N_s} \sum_{\mathbf{k_1}, \mathbf{k_2}} (e^{-i2k_x} + e^{i2k_x} - 2) \ll c_{\mathbf{k_1}}^{\dagger} c_{\mathbf{k_1}} \mid c_{\mathbf{k_2}}^{\dagger} c_{\mathbf{k_2}} \gg_{\omega}.
$$
(12)

Since the scattering process (or the interaction between bosons) in the BHK model preserves the momentum, $\hat{n}_k$ is a good quantum number, leading to $\ll c_{\mathbf{k_1}}^{\dagger} c_{\mathbf{k_1}} \mid c_{\mathbf{k_2}}^{\dagger} c_{\mathbf{k_2}} \gg_{\omega} = 0$. Therefore, for any μ/U and W/U, the current-current correlation function is invariant as zero. The Drude weight satisfies $\frac{D}{\pi e^2} = \langle -K_x \rangle$. Therefore, the bosons transport without dissipation, and the conductivity is completely determined by the average kinetic energy.

Next we consider the SF weight in the opposite limitation. In the BHK model, the effect of interaction has been accounted in the nontrivial distribution function $\langle \hat{n}_k \rangle$, while eigenstates retain a Fock-like form. Thus, the current-current correlation function can be expressed as

$$
\chi_{j_x j_x}(\mathbf{q} \to \mathbf{0}, \omega = 0)
$$

$$
= \frac{t^2}{N_s} \sum_{\mathbf{k_1}, \mathbf{k_2}} (e^{-i2k_x} + e^{i2k_x} - 2) \ll c_{\mathbf{k_1}}^{\dagger} c_{\mathbf{k_1}+\mathbf{q}} \mid c_{\mathbf{k_2}}^{\dagger} c_{\mathbf{k_2}-\mathbf{q}} \gg_{\omega=0}
$$

$$
= -\frac{t^2}{N_s} \sum_{\mathbf{k_1}, \mathbf{k_2}} (e^{-i2k_x} + e^{i2k_x} - 2) \delta_{\mathbf{k_2}, \mathbf{k_1}+\mathbf{q}} \frac{n_{\mathbf{k_1}+\mathbf{q}} - n_{\mathbf{k_1}}}{-\epsilon_{\mathbf{k_1}+\mathbf{q}} + \epsilon_{\mathbf{k_1}}}.
$$
(13)

For metallic states, the Drude weight D must be nonzero while insulators have $D = 0$. Furthermore, to identify SF states from generic metallic states, one expects that SF states with SF weight $D_s \neq 0$ and $D \neq 0$. (See also Table I.) Based on this prescription, in this paper, we will find that BHK model have BM and MI states but no SF (Fig. 4, see below).

C. Charge susceptibility

In addition to directly calculating the partial derivative of the particle number with respect to the chemical potential,

TABLE I. The Drude weight and SF weight for different states.

Variable	State BM	MI	SF
D_s	0	0	$\neq 0$
D	$\neq 0$	0	$\neq 0$

the charge susceptibility χ_c can also be obtained through the density-density correlation function. This correlation function, denoted as $\chi_c(\mathbf{R_i}, \mathbf{R_j}, t)$, is defined as the time-ordered commutator between the particle density operator $\hat{n}_i$ at site $\mathbf{R_i}$ and the particle density operator $\hat{n}_j$ at site $\mathbf{R_j}$. It can be expressed as follows:

$$
\chi_c(\mathbf{R_i}, \mathbf{R_j}, t) = -i\theta(t) \langle [\hat{n}_i(t), \hat{n}_j] \rangle
$$

$$
= \frac{-i}{N_s^2} \sum_{\mathbf{k_1}, \mathbf{k_2}, \mathbf{k_3}, \mathbf{k_4}} e^{-i(\mathbf{k_1}-\mathbf{k_2})\mathbf{R_i}} e^{-i(\mathbf{k_3}-\mathbf{k_4})\mathbf{R_j}}
$$

$$
\times \theta(t) \langle [\hat{c}_{\mathbf{k_1}}^{\dagger}(t) \hat{c}_{\mathbf{k_2}}(t), \hat{c}_{\mathbf{k_3}}^{\dagger} \hat{c}_{\mathbf{k_4}}] \rangle. \quad (14)
$$

This expression can be further transformed into momentum and frequency space using Fourier transformation,

$$
\chi_c(\mathbf{q}, \omega) = \frac{1}{N_s} \sum_{\mathbf{R_i}, \mathbf{R_j}} e^{-i\mathbf{q}(\mathbf{R_i}-\mathbf{R_j})} \int_0^{\infty} dt\, e^{i\omega t} \chi_c(\mathbf{R_i}, \mathbf{R_j}, t)
$$

$$
= \frac{1}{N_s} \sum_{\mathbf{k_1}, \mathbf{k_3}} \ll c_{\mathbf{k_1}}^{\dagger} c_{\mathbf{k_1}+\mathbf{q}} \mid c_{\mathbf{k_3}}^{\dagger} c_{\mathbf{k_3}-\mathbf{q}} \gg_{\omega}. \quad (15)
$$

The (static and uniform) charge susceptibility, which serves as an indicator of the phase boundary, is defined as the retarded Green's function at the zero-momentum and zero-frequency limit, i.e., $\chi_c = \chi_c(\mathbf{q} \to \mathbf{0}, \omega = 0) = \frac{1}{N_s} \frac{\partial N}{\partial \mu}$.

III. RESULTS

A. The ground-state phase diagram

Before delving into the intricacies of our calculations, we present our key finding encapsulated in the zero-temperature phase diagram (plotted on the $\mu - W$ plane), applicable to any spatial dimension (see Fig. 1). Here, $W = 4td$ represents the bandwidth of a hypercubic lattice with nearest-neighbor hopping. Our analysis reveals that the BHK system is predominantly governed by two distinct states: the MI state characterized by an integer density, and the BM state exhibiting varying densities. We emphasize that the MI state exhibits the greatest stability at each $\mu/U = \frac{2n-1}{2}$ (where n is an integer denoting the number density), wherein the boson density remains invariant with changing bandwidth. In this situation, the fixed-density MI-BM transition (or interaction-driven MI-BM transition) occurs at $U_c = W$. In the subsequent sections, we focus primarily on discussing specific parameter values, including one MI state ($W/U = 0.5, \mu/U = 0.5$) and three BM states ($W/U = 2, \mu/U = 0.5$, $W/U = 1, \mu/U = 2$, and $W/U = 2, \mu/U = 2.5$). For visual guidance, these specific points are marked with hexagonal symbols in Fig. 1.

We would like to emphasize a significant departure from the original study of the BHK model [4], wherein our findings reveal a remarkable substitution of the SF state with an
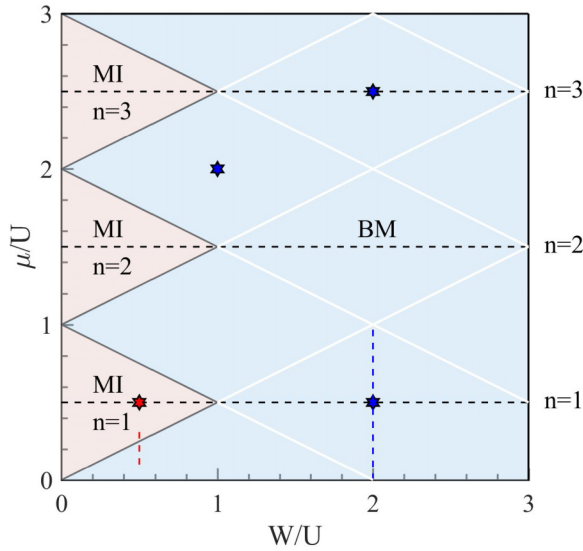
FIG. 1. The zero-temperature phase diagram of the Bose Hastugai-Khonmoto (BHK) model for any dimension. The phase diagram consists of the Mott insulator (MI) region (shown in red) at small W/U and the Bose metal (BM) region (shown in blue) at large W/U. Three red triangle regimes correspond to the MI states with different boson densities n, where $n = 1, 2, 3$ from bottom to top. The black line represents the Lifshitz transition between the MI and BM phases, while the white line denotes the Lifshitz transition between different BM states. The black dashed lines represent the state with an invariant integer boson density. The specific MI/BM state we focus in the latter of this paper is denoted by red/blue hexagon. The scaling behavior of the BM-MI phase transition along the red dashed line is demonstrated in Fig. 6, while the thermodynamic properties of the BM state along the blue dashed line are shown in Fig. 7.

unexpected BM state for any finite interaction strength U. Consequently, in the case of integer boson filling, our results demonstrate an MI-BM transition instead of the anticipated MI-SF transition as the interaction strength is increased. The precise reasons for the erroneous identification of the SF state by the authors in Ref. [4] remain elusive to us. However, it is worth noting that their study lacks any discernible calculations pertaining to charge susceptibility, SF weight, and Drude weight.

B. Mott insulator

The MI state here occurs when the number of bosons N is commensurate with the number of lattice sites N_s, i.e., $n = N/N_s = 1, 2, 3...$. Guided by Eq. (5), it is clear that the wavefunction of the MI state is given by

$$|\Psi_{\text{Mott}}\rangle = \prod_{k \in \text{BZ}} |n\rangle_k, \qquad (16)$$

where all momentum states are occupied by the same number of bosons, denoted as n. This argument is supported by the distribution function of bosons $\langle \hat{n}_k \rangle$, shown in Figs. 2(a) and 3(a), for the 1D chain and the 2D square lattice, respectively. The particle and hole excitation above $|\Psi_{\text{Mott}}\rangle$ can be constructed as $\hat{c}_q^\dagger |\Psi_{\text{Mott}}\rangle$, $\hat{c}_q |\Psi_{\text{Mott}}\rangle$, whose excitation energy are denoted as $\omega_p = \varepsilon_q + Un - \mu$, $\omega_h = -\varepsilon_q - U(n-1) + \mu$.
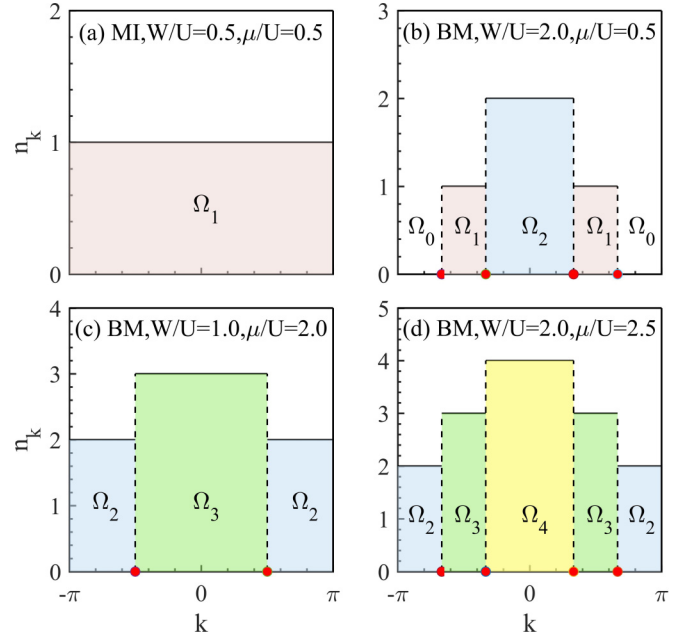

FIG. 2. Boson's distribution function $\langle \hat{n}_k \rangle$ in the one-dimensional BHK model for (a) the MI $W/U = 0.5$, $\mu/U = 0.5$; (b) the BM $W/U = 2$, $\mu/U = 0.5$; (c) the BM $W/U = 1$, $\mu/U = 2$; and (d) the BM $W/U = 2$, $\mu/U = 2.5$. The occupation number n in different momentum regimes is denoted by Ω_n. The Bose surface (gapless point) is denoted by the red circle, located at the step of the distribution function.

The stability of MI requires $\omega_p, \omega_h > 0$ for any momentum q, thus we can establish the MI regime in the ground state, which has been plotted in Fig. 1. To be specific, for given n, we have $\omega_p = \varepsilon_k + Un - \mu$, $\omega_h = \mu - \varepsilon_k - U(n-1)$. Then,
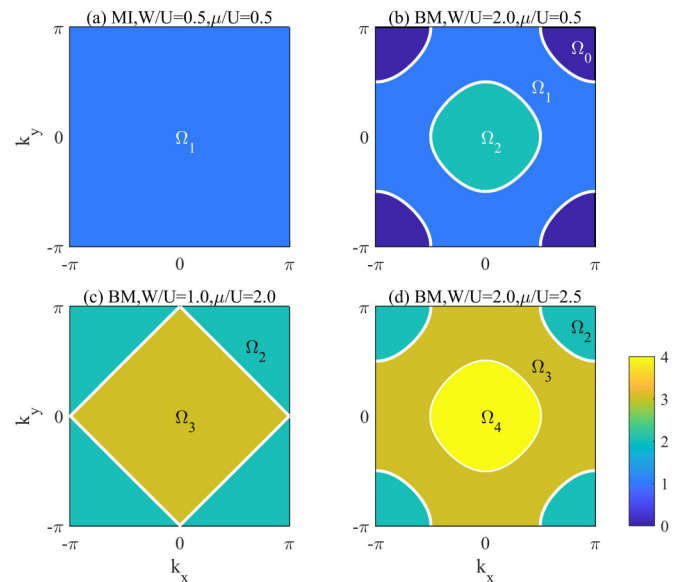

FIG. 3. Boson's distribution function $\langle \hat{n}_k \rangle$ in the two-dimensional BHK model for (a) the MI $W/U = 0.5$, $\mu/U = 0.5$; (b) the BM $W/U = 2$, $\mu/U = 0.5$; (c) the BM $W/U = 1$, $\mu/U = 2$; (d) the BM $W/U = 2$, $\mu/U = 2.5$. The Bose surface is denoted by write circle. Zero-energy excitation is located at the intersection of different Ω_n region.
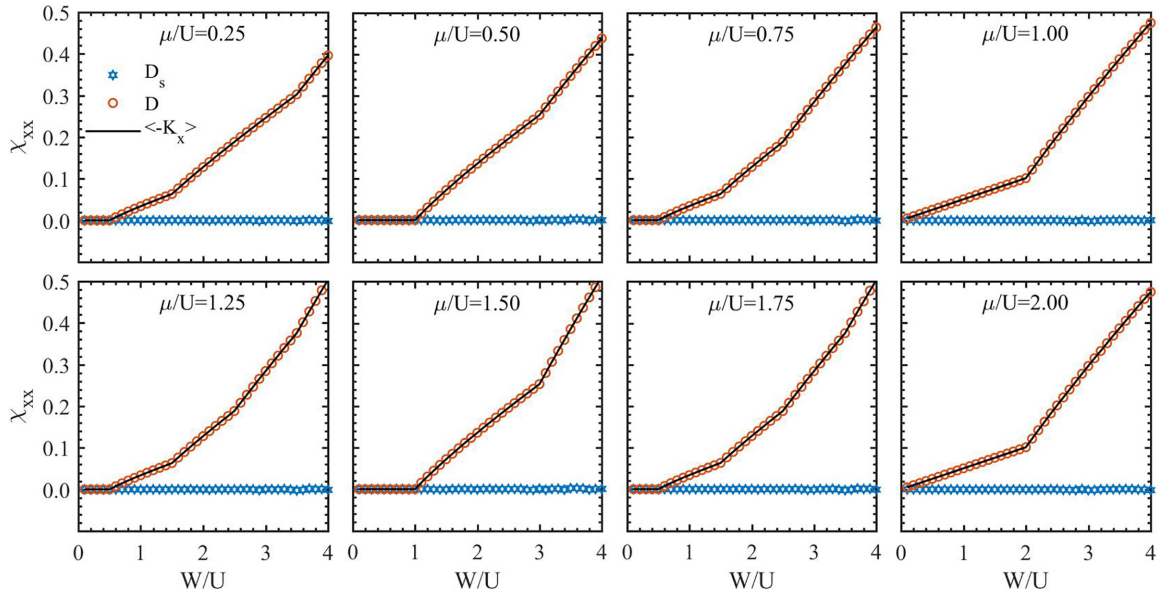
FIG. 4. The superfluid weight D_s (blue hexagon) and the Drude weight D (red star) in the two-dimensional BHK model for different chemical potential μ/U with varying W/U. The black line denotes minus kinetic energy per site divided by lattice dimension. The superfluid weight is invariant zero for both MI and BM states. The Drude weight is equal to $\langle -k_x \rangle$, indicating that no resistivity is caused by the HK interaction.

$\omega_p \to 0^+$ gives

$$\frac{\mu}{U} = \frac{(\varepsilon_k)_{\min}}{U} + n,$$

while $\omega_h \to 0^+$ gives

$$\frac{\mu}{U} = \frac{(\varepsilon_k)_{\max}}{U} + n - 1.$$

Here, $(\varepsilon_k)_{\min}$ and $(\varepsilon_k)_{\max}$ refer to the energy of the band bottom and top of the free bosons, respectively. Since $(\varepsilon_k)_{\min} =$

$-W/2$ and $(\varepsilon_k)_{\max} = W/2$. The above two equations plus $W/U = 0$ axis give us the regime of MI as shown in Fig. 1.

Because, $\omega_p, \omega_h > 0$ in MI, the charge susceptibility has to be vanished, i.e., $\chi_c = \frac{1}{N_s} \frac{\partial N}{\partial \mu} = 0$, which is the key signature of the insulating nature of MI. With the same reason, both Drude weight D and SF weight D_s are zero in MI (Fig. 4).

Furthermore, as evident from the spectral function $A(\omega, k)$ at zero temperature, Fig. 5(a) with momenta chosen along the path from $(-\pi, -\pi \dots -\pi)$ to $(0,0,..0)$ and to $(\pi, \pi \dots \pi)$, the MI state is characterized by a full-filled band [the dominated negative weight of $A(\omega, k)$]. For any given k, a finite energy is required for a boson to be excited or removed, which is consistent with the analysis of the wavefunction and the requirement of $\omega_p, \omega_h > 0$.

C. Bose metal

We have seen that the stability of MI leads to $\omega_p, \omega_h > 0$, otherwise, the gap for the particle and/or hole excitation can be vanished and MI must break down in this case. Our objective is to investigate the potential states that emerge when the breakdown of the MI occurs.

For those familiar with the BH model and Bogoliubov's SF theory, the SF state emerges as a highly plausible candidate in this context. It is well established that in the SF state, bosons tend to condense into a single momentum point, i.e., the condensation momentum k_0. For the dispersion $\epsilon_k = -2t \sum_{i=1}^{d} \cos k_i$, we find that $k_0 = (0, 0, ...0)$, i.e., the bottom of ϵ_k. The condensation in $| k_0 \rangle$ yields a SF wavefunction like $(\hat{c}_{k_0}^+)^N |0, 0, 0...\rangle = |N\rangle_{k_0}$. However, in contrast to SF, bosons in the BHK model do not condense into k_0 owing to the energy penalty from HK interactions. This significant difference between the SF state and our calculations is depicted in Figs. 2(b)–2(d) and 3(b)–3(d). Analogous to the Fermi surfaces in Fermi liquid/gas, distinct surfaces separate regimes
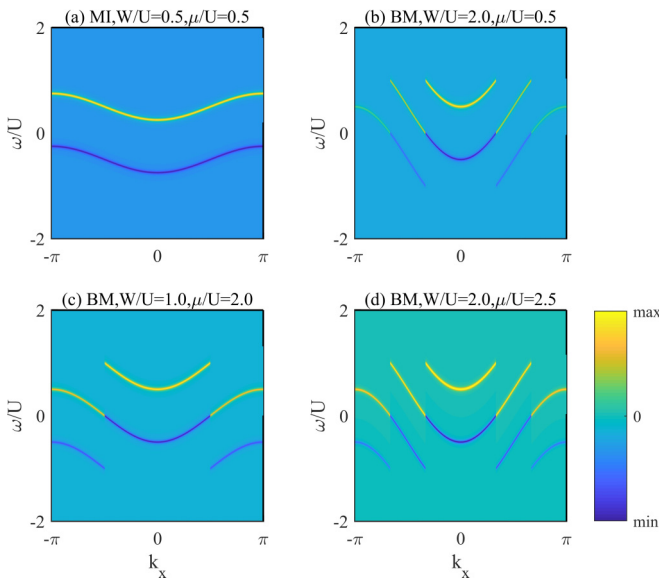

FIG. 5. The spectral function of the BHK model for (a) the MI $W/U = 0.5$, $\mu/U = 0.5$; (b) the BM $W/U = 2$, $\mu/U = 0.5$; (c) the BM $W/U = 1$, $\mu/U = 2$; and (d) the BM $W/U = 2$, $\mu/U = 2.5$.

with different particle numbers (Ω_n). We refer to these gapless surfaces as the "Bose surfaces", and to the states with Bose surfaces as the BM state.

The Bose surfaces live at discrete momentum points [indicated by red solid circles in Figs. 2(b)–2(d)] in one dimension, and it is more appropriate to term these points as Bose points, similar to their counterpart, i.e., the Fermi point in a one-dimensional Fermi liquid. In the case of a two-dimensional square lattice, the Bose surfaces form closed loops [represented as white lines in Figs. 3(b)–3(d)], akin to typical Fermi surfaces on a square lattice.

Let us consider a simple example. For Fig. 2(b), there are two pairs of Bose points and are denoted as $\pm k_{01}, \pm k_{12}$, which separates regimes with $\langle \hat{n}_k \rangle = 0, 1$ and $\langle \hat{n}_k \rangle = 1, 2$, respectively. Now, if we consider correlation function or single-particle density matrix $\langle c_i^\dagger c_j \rangle$, it is found that

$$
\begin{aligned}
\langle c_i^\dagger c_j \rangle &= \frac{1}{N_s} \sum_k e^{-ik(R_i - R_j)} \langle \hat{n}_k \rangle \\
&= \left(\int_{-k_{01}}^{-k_{12}} + \int_{k_{12}}^{k_{01}} \right) \frac{dk}{2\pi} e^{-ik(R_i - R_j)} \\
&\quad + \int_{-k_{12}}^{k_{12}} \frac{dk}{2\pi} 2 e^{-ik(R_i - R_j)} \\
&= \frac{2}{2\pi} \frac{\sin k_{01}(R_i - R_j) + \sin k_{12}(R_i - R_j)}{R_i - R_j},
\end{aligned}
$$

which just like the case of a free fermion system with Fermi wavevector k_{01}, k_{12}. In other words, if we add a nonmagnetic impurity into BHK model, we will expect that there exists a Friedel oscillation with characteristic wavevector k_{01} and k_{12} [69]. This may provide a practical approach to detect the Bose point or the generic Bose surface if they indeed exist. Moreover, when $|R_i - R_j| \to \infty$, we see $\langle c_i^\dagger c_j \rangle \to 0$ so SF-like long-ranged order for boson does not exist in the BM state. Such fact is valid for all spatial dimension and for all $U > 0$. In addition, we note that when $R_i = R_j$, the boson's density is $(2k_{01} + 2k_{12})/(2\pi)$, which acts as a Luttinger theorem for BM states [87].

To gain further insight into the behavior of the BM, MI, or SF in the BHK model, we examine the Drude weight D and SF weight D_s, as depicted in Fig. 4 [85,88]. In the presence of a nonzero SF and Drude weight ($D_s \neq 0, D \neq 0$), an SF state is expected. Conversely, a metal is characterized by a zero SF weight and a nonzero Drude weight ($D_s = 0, D \neq 0$). When both the SF and Drude weight vanish ($D_s = 0, D = 0$), it indicates the presence of an MI state. Figure 4 presents the variations of D (represented by red stars) and D_s (represented by blue hexagons) for different μ/U values with varying bandwidth W/U. As a reference, the diamagnetic response term, i.e., the minus total kinetic energy per dimension $\langle -K_x \rangle$, is plotted as a black line. For small values of W/U, the MI state is confirmed, as evidenced by the vanishing values of both D and D_s. As W/U increases, the SF weight D_s remains zero, while the Drude weight D grows at some critical W_c, which is consistent with the evolution of the structure of the momentum distribution during the MI-BM transition. The persistent absence of SF weight across different parameter regimes further confirms the absence of the SF state within

the finite-U regime. Associated with the unique distribution function, we conclude that the BM states prevail over the SF state in the metallic regimes of the BHK model.

Furthermore, we present the spectral function of the BM states in Figs. 5(b)–5(d). In this context, the yellow (blue) line represents the first (second) term in Eq. (6), which signifies the single-particle (single-hole) excitation. Within the single-particle spectrum, the Bose surface corresponds to the points where the spectral function undergoes continuous sign changes within a single band. Similar to the Fermi liquid, the MI and BM can also be distinguished by the absence or presence of a Bose surface. In the MI state, where chemical potential resides within the energy gap [as depicted in Fig. 5(a)], no Bose surface is observed. Conversely, the BM states can exhibit multiple Bose surfaces, as illustrated in Figs. 5(b)–5(d).

D. The Lifshitz transition

To elucidate the putative phase transition in the BHK model, we begin by plotting the global charge susceptibility in the W-μ plane for a one-dimensional system [see Fig. 6(a)]. The divergent χ_c delineates the phase boundary between distinct states, which can be expressed as

$$
\mu_{c1} = (n - 1)U + \frac{W}{2},
$$
$$
\text{or} \qquad (17)
$$
$$
\mu_{c2} = nU - \frac{W}{2},
$$

where $n = 1, 2, \dots$. Notably, μ_{c1} and μ_{c2} corresponds precisely to the the top and bottom of the nth band, respectively. Based on the location of divergence and the evolution of $\langle \hat{n}_k \rangle$ discussed earlier, we anticipate that these zero-temperature quantum transitions are connected to Lifshitz transitions [86]. For a d-dimensional system near the Lifshitz transition point, the dynamical critical exponents z, the correlation length exponent ν, and the critical exponent α should satisfy $z = 2$, $\nu = 1/2$, $\alpha = 1 - d/2$, respectively. In conventional, $g = \mu - \mu_c$ is the natural variable for Lifshitz transitions, signifying the distance of the chemical potential μ from the band top or bottom. To verify this conjecture for our BHK model, we study the scaling behavior of the free energy density f, the particle density n, and the charge susceptibility χ_c around the phase transition, which should follow

$$
\begin{aligned}
\Delta f &= f - f_0 \sim (\mu - \mu_c)^{d/2+1}, \\
\Delta n &= n - n_0 \sim (\mu - \mu_c)^{d/2}, \\
\Delta \chi &= \chi - \chi_0 \sim (\mu - \mu_c)^{d/2-1}. \quad (18)
\end{aligned}
$$

Here, f_0, n_0, and χ_0 represent certain background values that need to be subtracted. For free energy density ($f = E - \mu n$), the chemical potential energy is subtracted to avoid the influence of the linear term $n(\mu - \mu_c)$. We now focus on the specific case $W/U = 0.5$ around $\mu_{c2}/U = 0.25$, where the critical chemical potential of the BM-MI transition locates on the top of the lowest band. As illustrated in Figs. 6(b)–6(d), we examine the scaling behavior of the quantum phase transition for different dimensions ($d = 1, 2, 3$). It is evident that in the
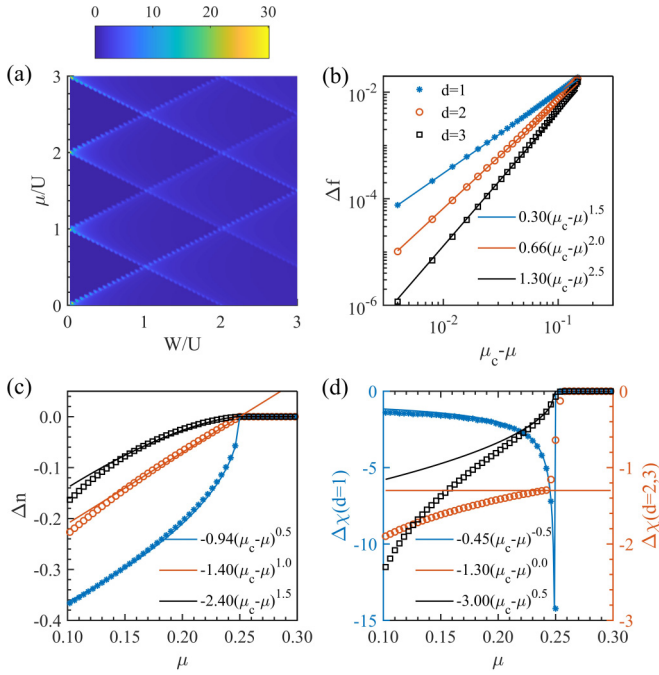
FIG. 6. (a) The charge susceptibility χ_c evaluated on the W-μ plane for a $d = 1$ BHK system. The calculations are performed on a lattice with $N_s = 40\,000$ sites, and the obtained results are qualitatively consistent with those expected in higher-dimensional scenarios. (b) Free energy density, (c) particle density, and (d) charge susceptibility around critical point $\mu_c = 0.25$ vs fitted scaling formula (18) with $W/U = 0.5$.

metallic regime, f, n, and χ_c all exhibit behavior consistent with the critical exponents of the Lifshitz transition. It is worth noting that varying the bandwidth at a fixed chemical potential also induces transitions by changing the variable $\mu - \mu_c$. Consequently, we conclude that both the chemical potential-driven and bandwidth-driven BM-MI transitions are manifestations of the Lifshitz transition. Such feature seems to be general for HK-like models [4,68].

IV. FINITE-TEMPERATURE PROPERTIES

In this section, we investigate the heat capacity and the charge susceptibility at finite temperature. Using the basis given in Eq. (4) and the energy spectrum, we can easily calculate the averages of observables using the partition function. For instance, the energy can be expressed as

$$E = \langle \hat{H} \rangle = \sum_n \frac{1}{\mathcal{Z}} e^{-\beta E_n} \langle n | \hat{H} | n \rangle. \quad (19)$$

As shown in Fig. 7(a), the heat capacity in the BM state exhibits a clear linear dependence on temperature, which is consistent with the behavior of a Fermi liquid ($Cv \sim \gamma T$). A similar situation is observed for the charge susceptibility χ_c. In the BM states, χ_c saturates around zero temperature [$\chi_c(T \to 0) = c$]. The constant c shows a linear dependence on the particle density around the Bose surface [$c \sim N(0)$], as shown in Fig. 7(b). In a Fermi liquid, $N(0)$ represents the particle density around the Fermi surface. Note that at $\mu/U = 0, 1$, Cv deviates from the linear temperature dependence.
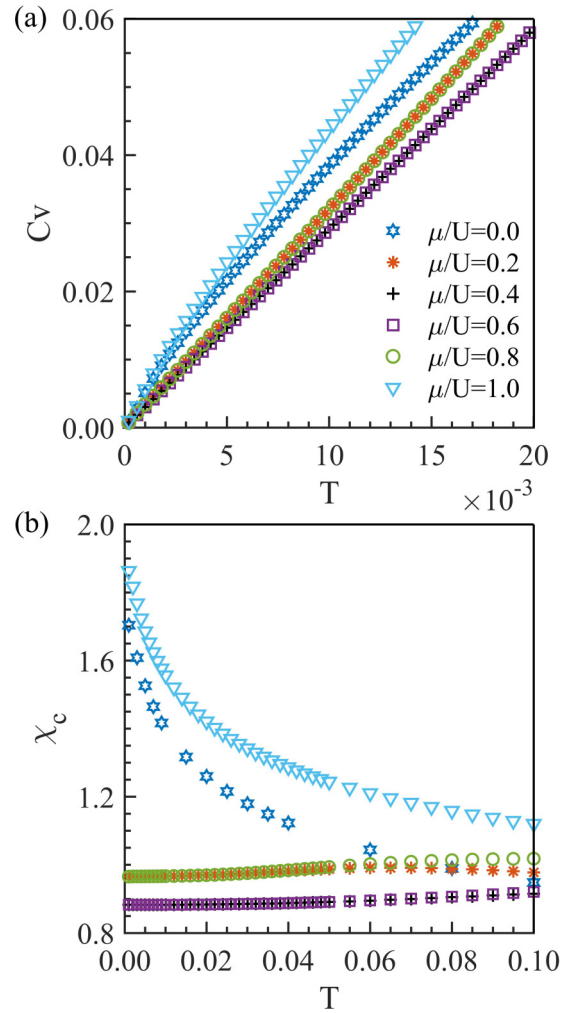

FIG. 7. (a) The heat capacity Cv and (b) the charge susceptibility χ_c vs temperature with various chemical potential μ at $W/U = 2$ in the BM state. Except for the situation $\mu/U = 0, 1, ..., Cv$ demonstrates a linear dependence when approaching zeros temperature, while χ_c is a constant number proportional to $N(0)$.

dence, and there is no saturation signal for χ_c at $T \to 0$ limit. This deviation in the thermodynamic properties from the behavior of a Fermi liquid corresponds to the critical point of the Lifshitz transition between different BM states that we discussed earlier.

V. DISCUSSION

A. Comparison with the Bose-Hubbard model

In the BH model, a similar phase diagram is reported, where the MI state manifests in lobes with an integer boson density [3,89,90]. Here, we compare the properties of the MI and BM states in the BHK model with the MI and SF states in the BH model.

In both the BH and the BHK model, the MI state in the lobes is characterized by a finite energy gap to all excitations with no broken translation symmetry. The total boson number N is invariant under changes of chemical potential $\frac{\partial \langle \hat{N} \rangle}{\partial \mu} = 0$, demonstrating the incompressibility of the MI state.
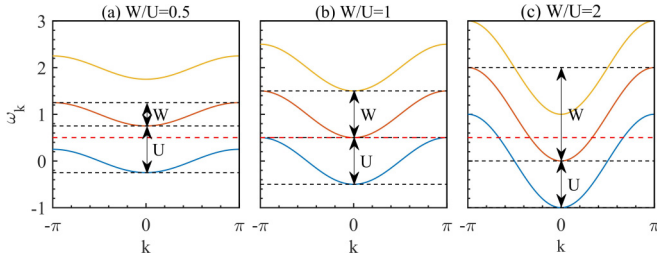
FIG. 8. The schematic picture of the three lowest bands for (a) $W/U = 0.5$; (b) the critical point $W_c/U = 1$ (for the disappearing of MI state); (c) $W/U = 2$. The chemical potential $\mu/U = 0.5$ is denoted by red dashed line.

Figure 8 depicts the schematic band structure of the BHK model. The MI state exists only for $W/U < 1$, where the chemical potential lies within the energy gap (see Fig. 8). The BHK system become compressible with the MI-BM transition. However, the robust direct gap existing in both MI and BM states yields the incompressibility of each independent $|k\rangle$ state, i.e., $\frac{\partial \langle \hat{n}_k \rangle}{\partial \mu} \neq 0$. This precludes the SF, which relies on gapless excitations of the $|k_0\rangle$ state in the BH model. Thus, we conclude that the BM is a metallic state with compressible wavefunction and incompressible $|k_0\rangle$ state, distinguishing it from the SF state.

B. Why BM state like Fermi liquid

We have observed that the metallic states in BHK model, namely the BM state looks like the usual Fermi liquid because the former exhibits the linear-T specific heat and nonzero χ_c. To gain a more intuitive understanding of this phenomenon, let us consider the limit $U \to \infty$ limit. (Note that this limit has been addressed in the framework of superexclusion statistics theory [70], and our analysis is in line with this theory. In the case of infinite U, the system is characterized by the presence of only empty and singly occupied states, which corresponds to the situation that the spinless fermions have the same statistics as the hardcore bosons.) In this scenario, the summation over n_k in partition function $\mathcal{Z} = \prod_k \sum_{n_k=0}^{\infty} e^{-\beta E_{n_k}}$ is truncated to $n_k = 1$. Consequently, we find $\mathcal{Z} = \prod_k (1 + e^{-\beta(\varepsilon_k - \mu)})$ and its free energy is given by $F = -T \sum_k \ln(1 + e^{-\beta(\varepsilon_k - \mu)})$. This corresponds to a free fermion gas with dispersion ε_k. So, $Cv \sim T$, $\chi_c \sim$ constant has been explained.

Furthermore, in the $U \to \infty$ limit, the value of n_k is either zero or one. For regimes where $n_k = 0$, the Green's function only includes particle excitations, given by

$$G^R(\omega, k) = \frac{1}{\omega - (\varepsilon_k - \mu)}, \qquad (20)$$

while for regimes where $n_k = 1$, only hole excitations exist, described by

$$G^R(\omega, k) = -\frac{1}{\omega - (\varepsilon_k - \mu)}. \qquad (21)$$

It is interesting to note that the above Green's functions correspond to free fermion's counterpart, although the hole excitation in the BM state carries an additional minus sign. This sign is necessary to ensure causality in the retarded Green's function of any boson.

Finally, since the ground states of the BHK model are all product states characterized by the occupation of each momentum k, and in the $U \to \infty$ limit, the state with $n_k = 0$ ($n_k = 1$) has energy 0 ($\varepsilon_k - \mu$), there exist boundaries ($\varepsilon_k - \mu = 0$) that separate unoccupied and occupied states. These boundaries serve as the Fermi surface and are the expected Bose surface in our model.

VI. CONCLUSIONS

In conclusion, our study has uncovered a MI-BM transition in the exactly solvable BHK model, which falls under the universality class of the Lifshitz transition. The existence of the BM state is supported by the distinct momentum distribution function, the presence of a finite Drude weight, and the absence of SF weight. At low temperatures, the BM state exhibits a linear-T-dependent heat capacity and a saturate charge susceptibility, demonstrating behavior akin to a Fermi liquid. Comparing the BM state with the SF state observed in the BH model, we conclude that the BM state is characterized by a compressible total wavefunction and an incompressible zero-momentum component.

Importantly, our paper presents a promising approach to realize this exotic BM state. It is indicated that any finite infinite-range interaction can disrupt the SF state, which aligns with the conventional notion that nontrivial long-range interaction is crucial for accessing the BM state. The contrasting nature between long-ranged and short-ranged interactions is clearly demonstrated in the different phase diagram in the BHK model with infinite-range interaction and the BH model with on-site interaction, leading to distinct stable phases with weak interaction, namely the BM state and the SF state, respectively. In some sense, the infinite-range HK interaction just frustrates bosons in momentum space, thus bosons are not likely to condensate into any particular momentum and no SF forms.

However, we note that the BHK model studied here cannot give finite resistivity at finite temperature, which has been observed in experiments on boson metals, since no disorder or impurity effect is included. But, it is also noted that the existence of our BM states do nor require external magnetic field, disorder or fine tuning of carrier density, thus BM states could be a robust state of matter, which is stabilized by nontrivial HK interaction. Therefore, we believe that the study of HK-like models is indeed an important direction in the many-body physics and many more interesting physics will be discovered when complicated details are included.

[1] A. Fetter and J. Walecka, *Quantum Theory of Many-Particle Systems*, Dover Books on Physics (Dover Publications, New York, 2003).

[2] M. Greiner, O. Mandel, T. Esslinger, T. W. Hänsch, and I. Bloch, Nature (London) **415**, 39 (2002).

[3] S. Sachdev, *Quantum Phases of Matter* (Cambridge University Press, Cambridge, 2023).

[4] M. A. Continentino and M. D. Coutinho-Filho, Solid State Commun. **90**, 619 (1994).

[5] M. P. A. Fisher, P. B. Weichman, G. Grinstein, and D. S. Fisher, Phys. Rev. B **40**, 546 (1989).

[6] E. Abrahams, P. W. Anderson, D. C. Licciardello, and T. V. Ramakrishnan, Phys. Rev. Lett. **42**, 673 (1979).

[7] H. M. Jaeger, D. B. Haviland, B. G. Orr, and A. M. Goldman, Phys. Rev. B **40**, 182 (1989).

[8] D. Ephron, A. Yazdani, A. Kapitulnik, and M. R. Beasley, Phys. Rev. Lett. **76**, 1529 (1996).

[9] N. Mason and A. Kapitulnik, Phys. Rev. Lett. **82**, 5341 (1999).

[10] C. Christiansen, L. M. Hernandez, and A. M. Goldman, Phys. Rev. Lett. **88**, 037004 (2002).

[11] S. Eley, S. Gopalakrishnan, P. M. Goldbart, and N. Mason, Nat. Phys. **8**, 59 (2012).

[12] W. Liu, L. D. Pan, J. Wen, M. Kim, G. Sambandamurthy, and N. P. Armitage, Phys. Rev. Lett. **111**, 067003 (2013).

[13] J. Garcia-Barriocanal, A. Kobrinskii, X. Leng, J. Kinney, B. Yang, S. Snyder, and A. M. Goldman, Phys. Rev. B **87**, 024509 (2013).

[14] Z. Han, A. Allain, H. Arjmandi-Tash, K. Tikhonov, M. Feigel'man, B. Sacépé, and V. Bouchiat, Nat. Phys. **10**, 380 (2014).

[15] Y. Saito, Y. Kasahara, J. Ye, Y. Iwasa, and T. Nojima, Science **350**, 409 (2015).

[16] N. P. Breznay and A. Kapitulnik, Sci. Adv. **3**, e1700612 (2017).

[17] A. Kapitulnik, S. A. Kivelson, and B. Spivak, Rev. Mod. Phys. **91**, 011002 (2019).

[18] C. G. L. Bøttcher, F. Nichele, M. Kjaergaard, H. J. Suominen, J. Shabani, C. J. Palmstrøm, and C. M. Marcus, Nat. Phys. **14**, 1138 (2018).

[19] Z. Chen, A. G. Swartz, H. Yoon, H. Inoue, T. A. Merz, D. Lu, Y. Xie, H. Yuan, Y. Hikita, S. Raghu, and H. Y. Hwang, Nat. Commun. **9**, 4008 (2018).

[20] C. Yang, Y. Liu, Y. Wang, L. Feng, Q. He, J. Sun, Y. Tang, C. Wu, J. Xiong, W. Zhang *et al.*, Science **366**, 1505 (2019),.

[21] A. W. Tsen, B. Hunt, Y. D. Kim, Z. J. Yuan, S. Jia, R. J. Cava, J. Hone, P. Kim, C. R. Dean, and A. N. Pasupathy, Nat. Phys. **12**, 208 (2016).

[22] E. Shimshoni, A. Auerbach, and A. Kapitulnik, Phys. Rev. Lett. **80**, 3352 (1998).

[23] A. Kapitulnik, N. Mason, S. A. Kivelson, and S. Chakravarty, Phys. Rev. B **63**, 125322 (2001).

[24] V. M. Galitski, G. Refael, M. P. A. Fisher, and T. Senthil, Phys. Rev. Lett. **95**, 077002 (2005).

[25] D.-H. Lee, S. Kivelson, and S.-C. Zhang, Phys. Rev. Lett. **67**, 3302 (1991).

[26] D. Das and S. Doniach, Phys. Rev. B **60**, 1261 (1999).

[27] P. Phillips and D. Dalidovich, Science **302**, 243 (2003).

[28] B. Spivak, A. Zyuzin, and M. Hruska, Phys. Rev. B **64**, 132502 (2001).

[29] B. Spivak, P. Oreto, and S. A. Kivelson, Phys. Rev. B **77**, 214523 (2008).

[30] M. Mulligan and S. Raghu, Phys. Rev. B **93**, 205116 (2016).

[31] M. Feigel'man and A. Larkin, Chem. Phys. **235**, 107 (1998).

[32] D. Dalidovich and P. Phillips, Phys. Rev. Lett. **89**, 027001 (2002).

[33] J. Wu and P. Phillips, Phys. Rev. B **73**, 214507 (2006).

[34] R. A. Davison, L. V. Delacrétaz, B. Goutéraux, and S. A. Hartnoll, Phys. Rev. B **94**, 054502 (2016).

[35] D. Das and S. Doniach, Phys. Rev. B **64**, 134511 (2001).

[36] H. S. J. van der Zant, W. J. Elion, L. J. Geerligs, and J. E. Mooij, Phys. Rev. B **54**, 10081 (1996).

[37] Z. Chen, B. Y. Wang, A. G. Swartz, H. Yoon, Y. Hikita, S. Raghu, and H. Y. Hwang, npj Quantum Mater. **6**, 15 (2021).

[38] M. V. Feigelman, V. B. Geshkenbein, L. B. Ioffe, and A. I. Larkin, Phys. Rev. B **48**, 16641 (1993).

[39] O. I. Motrunich and M. P. A. Fisher, Phys. Rev. B **75**, 235116 (2007).

[40] D. Dalidovich and P. Phillips, Phys. Rev. B **64**, 052507 (2001).

[41] D. N. Sheng, O. I. Motrunich, S. Trebst, E. Gull, and M. P. A. Fisher, Phys. Rev. B **78**, 054520 (2008).

[42] M. S. Block, R. V. Mishmash, R. K. Kaul, D. N. Sheng, O. I. Motrunich, and M. P. A. Fisher, Phys. Rev. Lett. **106**, 046402 (2011).

[43] Y. Hatsugai and M. Kohmoto, J. Phys. Soc. Jpn. **61**, 2056 (1992).

[44] G. Baskaran, Mod. Phys. Lett. B **05**, 643 (1991).

[45] S. Sachdev and J. Ye, Phys. Rev. Lett. **70**, 3339 (1993).

[46] J. Maldacena and D. Stanford, Phys. Rev. D **94**, 106002 (2016).

[47] D. Chowdhury, A. Georges, O. Parcollet, and S. Sachdev, Rev. Mod. Phys. **94**, 035004 (2022).

[48] Y. Zhou, K. Kanoda, and T.-K. Ng, Rev. Mod. Phys. **89**, 025003 (2017).

[49] C. Prosko, S.-P. Lee, and J. Maciejko, Phys. Rev. B **96**, 205104 (2017).

[50] Y. Zhong, Y.-F. Wang, and H.-G. Luo, Phys. Rev. B **88**, 045109 (2013).

[51] A. Smith, J. Knolle, D. L. Kovrizhin, and R. Moessner, Phys. Rev. Lett. **118**, 266601 (2017).

[52] Z. Chen, X. Li, and T. K. Ng, Phys. Rev. Lett. **120**, 046401 (2018).

[53] A. Kitaev, Ann. Phys. **303**, 2 (2003).

[54] A. Kitaev, Ann. Phys. **321**, 2 (2006).

[55] Y. Hatsugai, M. Kohmoto, T. Koma, and Y.-S. Wu, Phys. Rev. B **54**, 5358 (1996).

[56] P. W. Phillips, C. Setty, and S. Zhang, Phys. Rev. B **97**, 195102 (2018).

[57] L. Yeo and P. W. Phillips, Phys. Rev. D **99**, 094030 (2019).

[58] H.-S. Zhu, Z. Li, Q. Han, and Z. D. Wang, Phys. Rev. B **103**, 024514 (2021).

[59] K. Yang, Phys. Rev. B **103**, 024529 (2021).

[60] J. Zhao, L. Yeo, E. W. Huang, and P. W. Phillips, Phys. Rev. B **105**, 184509 (2022).

[61] E. W. Huang, G. L. Nave, and P. W. Phillips, Nat. Phys. **18**, 511 (2022).

[62] P. Mai, B. E. Feldman, and P. W. Phillips, Phys. Rev. Res. **5**, 013162 (2023).

[63] Y. Li, V. Mishra, Y. Zhou, and F.-C. Zhang, New J. Phys. **24**, 103019 (2022).

[64] C. Setty, Phys. Rev. B **101**, 184506 (2020).

[65] C. Setty, Phys. Rev. B **103**, 014501 (2021).

[66] P. W. Phillips, L. Yeo, and E. W. Huang, Nat. Phys. **16**, 1175 (2020).

[67] C. Setty, arXiv:2105.15205.

[68] Y. Zhong, Phys. Rev. B **106**, 155119 (2022).

[69] M. Zhao, W.-W. Yang, H.-G. Luo, and Y. Zhong, J. Phys.: Condens. Matter **35**, 495603 (2023).

[70] J. Spalek and W. Wójcik, Phys. Rev. B **37**, 1532 (1988).

[71] K. Byczuk and J. Spalek, Phys. Rev. B **50**, 11403 (1994).

[72] K. Byczuk and J. Spalek, Phys. Rev. B **51**, 7934 (1995).

[73] E. J. Meier, F. A. An, A. Dauphin, M. Maffei, P. Massignan, T. L. Hughes, and B. Gadway, Science **362**, 929 (2018).

[74] B. Gadway, Phys. Rev. A **92**, 043606 (2015).

[75] E. J. Meier, F. A. An, and B. Gadway, Phys. Rev. A **93**, 051602(R) (2016).

[76] F. A. An, B. Sundar, J. Hou, X.-W. Luo, E. J. Meier, C. Zhang, K. R. A. Hazzard, and B. Gadway, Phys. Rev. Lett. **127**, 130401 (2021).

[77] R. Rosa-Medina, F. Ferri, F. Finger, N. Dogra, K. Kroeger, R. Lin, R. Chitra, T. Donner, and T. Esslinger, Phys. Rev. Lett. **128**, 143602 (2022).

[78] D. Xie, W. Gou, T. Xiao, B. Gadway, and B. Yan, npj Quantum Inf. **5**, 55 (2019).

[79] P. Lauria, W.-T. Kuo, N. R. Cooper, and J. T. Barreiro, Phys. Rev. Lett. **128**, 245301 (2022).

[80] Y. Wang, J.-H. Zhang, Y. Li, J. Wu, W. Liu, F. Mei, Y. Hu, L. Xiao, J. Ma, C. Chin, and S. Jia, Phys. Rev. Lett. **129**, 103401 (2022).

[81] H. Li, Z. Dong, S. Longhi, Q. Liang, D. Xie, and B. Yan, Phys. Rev. Lett. **129**, 220403 (2022).

[82] Z. Chen, H. Yao, E. Haber, and N. P. Bigelow, Phys. Rev. Res. **4**, 013124 (2022).

[83] J.-T. Wang and P. He, Phys. Rev. A **107**, 043321 (2023).

[84] B. Zeng, X. Chen, D.-L. Zhou, and X.-G. Wen, *Quantum Information Meets Quantum Matter* (Springer, New York, 2019).

[85] D. J. Scalapino, S. R. White, and S. C. Zhang, Phys. Rev. Lett. **68**, 2830 (1992).

[86] M. A. Continentino, *Quantum Scaling in Many-Body Systems: An Approach to Quantum Phase Transitions* (Cambridge University Press, Cambridge, 2017).

[87] C. Vitoriano, L. B. Bejan, A. M. S. Macêdo, and M. D. Coutinho-Filho, Phys. Rev. B **61**, 7941 (2000).

[88] P. Coleman, *Introduction to Many-Body Physics* (Cambridge University Press, Cambridge, 2015).

[89] F. Alet and E. S. Sørensen, Phys. Rev. B **70**, 024513 (2004).

[90] T. D. Kühner, S. R. White, and H. Monien, Phys. Rev. B **61**, 12474 (2000).